BIOLOGICAL CRYSTALLOGRAPHY

ISSN 1399-0047

Structural basis of *Deerpox virus*-mediated inhibition of apoptosis

Denis R. Burton,[a,b] Sofia Caria,[a,b] Bevan Marshall,[a,b] Michele Barry[c] and Marc Kvansakul[a,b]*

[a]Department of Biochemistry, La Trobe University, Melbourne, VIC 3058, Australia, [b]La Trobe Institute for Molecular Science, La Trobe University, Melbourne, VIC 3086, Australia, and [c]Li Ka Shing Institute for Virology, Department of Medical Microbiology and Immunology, University of Alberta, Edmonton, Alberta T6G 2S2, Canada. *Correspondence e-mail: m.kvansakul@latrobe.edu.au

Received 24 December 2014
Accepted 18 May 2015

Edited by C. S. Bond, University of Western Australia, Crawley, Australia

Keywords: apoptosis; Bcl-2; poxvirus; X-ray crystallography.

PDB references: *Deerpox virus* DPV022, complex with Bak BH3, 4uf1; complex with Bax BH3, 4uf2; complex with Bim BH3, 4uf3

Supporting information: this article has supporting information at journals.iucr.org/d

Apoptosis is a key innate defence mechanism to eliminate virally infected cells. To counteract premature host-cell apoptosis, poxviruses have evolved numerous molecular strategies, including the use of Bcl-2 proteins, to ensure their own survival. Here, it is reported that the *Deerpox virus* inhibitor of apoptosis, DPV022, only engages a highly restricted set of death-inducing Bcl-2 proteins, including Bim, Bax and Bak, with modest affinities. Structural analysis reveals that DPV022 adopts a Bcl-2 fold with a dimeric domain-swapped topology and binds pro-death Bcl-2 proteins *via* two conserved ligand-binding grooves found on opposite sides of the dimer. Structures of DPV022 bound to Bim, Bak and Bax BH3 domains reveal that a partial obstruction of the binding groove is likely to be responsible for the modest affinities of DPV022 for BH3 domains. These findings reveal that domain-swapped dimeric Bcl-2 folds are not unusual and may be found more widely in viruses. Furthermore, the modest affinities of DPV022 for pro-death Bcl-2 proteins suggest that two distinct classes of anti-apoptotic viral Bcl-2 proteins exist: those that are monomeric and tightly bind a range of death-inducing Bcl-2 proteins, and others such as DPV022 that are dimeric and only bind a very limited number of death-inducing Bcl-2 proteins with modest affinities.

1. Introduction

Programmed cell death, or apoptosis, is a critical mechanism to remove damaged, infected or unwanted cells in multi-cellular organisms (Youle & Strasser, 2008), and proteins of the Bcl-2 (B-cell lymphoma 2; Vaux *et al.*, 1988) family are the main regulators of apoptosis mediated by the intrinsic pathway (Adams & Cory, 1998). The Bcl-2 family is divided into anti-apoptotic and pro-apoptotic members, all of which share one or more of four conserved Bcl-2 homology (BH) domains (Kvansakul & Hinds, 2013*a*). Anti-apoptotic Bcl-2 proteins, including Bcl-2, Bcl-x_L, Bcl-w, Mcl-1, A1 and Bcl-b, block apoptosis. Pro-apoptotic Bcl-2 members are further subdivided into two groups, those that only harbour a BH3 domain, which are termed the BH3-only proteins, and the multi-BH domain proteins Bax, Bak and Bok (Chipuk *et al.*, 2010; Kvansakul & Hinds, 2013*b*). The BH3-only proteins, including Bim, Puma, Bad and Noxa, either directly activate pro-apoptotic Bax and Bak, or neutralize anti-apoptotic Bcl-2 members by engaging their receptor-binding groove using the α-helical BH3 domains (Shamas-Din *et al.*, 2011). Upon activation, Bax and Bak oligomerize to cause organellar damage

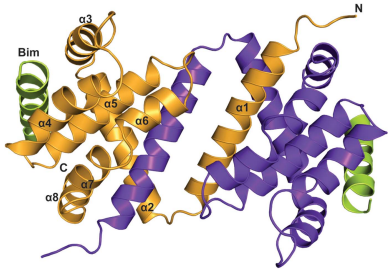

including permeabilization of the outer mitochondrial membrane (Chipuk & Green, 2008; Czabotar *et al.*, 2013), thus releasing critical pro-apoptogenic factors such as cytochrome *c* and SMAC/Diablo to enable the activation of caspases (Green & Kroemer, 2004).

Viruses have evolved multiple strategies to counter premature host-cell apoptosis, including the expression of virulence factors homologous to the Bcl-2 family of proteins (Galluzzi *et al.*, 2008). These viral Bcl-2-like proteins, including those expressed by adenovirus (White *et al.*, 1992), Kaposi's sarcoma-associated herpesvirus (KSHV; Cheng *et al.*, 1997), Epstein–Barr virus (EBV; Henderson *et al.*, 1993) and γ-herpesvirus 68 (Wang *et al.*, 1999), are all required for successful viral propagation and/or persistence (Altmann & Hammerschmidt, 2005). However, certain viruses, including members of the *Poxviridae*, express anti-apoptotic proteins that are unrelated in sequence to any other known cell-death regulator (Best, 2008). These proteins include *Myxoma virus* M11L (Graham *et al.*, 1992), *Vaccinia virus* (VACV) and *Variola virus* (VAR) F1L (Marshall *et al.*, 2014; Wasilenko *et al.*, 2003), VACV N1L (Bartlett *et al.*, 2002) and VACV E3L (Fischer *et al.*, 2005), and the more recently identified *Fowlpox virus* FPV039 (Banadyga *et al.*, 2007), *Orf virus* ORF125 (Westphal *et al.*, 2007) and *Sheeppox virus* SPPV14 (Okamoto *et al.*, 2012). Despite a lack of sequence similarity to Bcl-2 proteins, both M11L (Douglas *et al.*, 2007; Kvansakul *et al.*, 2007) and F1L (Kvansakul *et al.*, 2008) have been shown to adopt a Bcl-2 fold that is able to engage BH3 domains in a conserved ligand-binding groove. Furthermore, the engagement of pro-death proteins utilizing this groove is critical for successful subversion of apoptosis, with M11L operating primarily by sequestering Bax and Bak (Kvansakul *et al.*, 2007), whereas F1L relies on engagement of Bim to prevent apoptosis in the context of a live viral infection (Campbell *et al.*, 2014)

A search for other putative anti-apoptotic proteins in viruses using the sequence of M11L revealed the *Deerpox virus* open reading frame 22 (DPV022) as a protein with limited sequence identity that may harbour anti-apoptotic activity (Okamoto *et al.*, 2012). Functional and cellular studies revealed that DPV022 is indeed anti-apoptotic, localizes to the mitochondrial outer membrane and is able to directly engage Bax and Bak (Banadyga *et al.*, 2011). However, whether or not DPV022 is able to engage pro-apoptotic Bcl-2 proteins other than Bax and Bak is not clear. Similarly, the molecular and structural basis for the ability of DPV022 to inhibit apoptosis remains to be clarified. To address these issues, we systematically examined the interactions of DPV022 with BH3-domain peptides of pro-apoptotic Bcl-2 proteins and determined the crystal structures of DPV022 bound to the identified binding partners. Our analysis reveals that DPV022 harbours a highly restricted pro-apoptotic ligand-binding profile and only binds Bim, Bax and Bak with moderate affinities. Structural analysis reveals that DPV022 adopts a domain-swapped dimeric configuration, in which two independent ligand-binding grooves engage two pro-apoptotic ligands simultaneously. Furthermore, our findings suggest the existence of three discrete classes of viral Bcl-2 like proteins that can be distinguished based on their oligomeric state, range of pro-apoptotic ligands and associated affinities.

2. Materials and methods

2.1. Cloning, expression and purification

The codon-optimized cDNA of DPV022 (GenScript) was used to amplify the region coding for residues 1–155 of DPV022 (referred to as DPV022ΔC24 to indicate the removal of the transmembrane domain; Fig. 4), cloned into the pETDuet vector (Invitrogen) using an introduced 5′ BamHI restriction site and 3′ EcoRI site followed by a stop codon, and expressed in *Escherichia coli* BL21(DE3) pLysS cells. This led to the addition of an MGSSHHHHHHSQDP sequence at the native N-terminus of the protein. Cells were grown in 2YT medium containing 1 mg ml^{-1} ampicillin at 310 K in a shaker incubator operating at 160 rev min^{-1} until an OD_{600} of 0.6 was reached. Protein expression was induced for 4 h by the addition of isopropyl β-D-1-thiogalactopyranoside (IPTG) to the culture at a final concentration of 1 m*M*. The cells were harvested by centrifugation at 4000 rev min^{-1} (JLA 9.1000 rotor, Beckman Coulter Avanti J-E) for 15 min and resuspended in 40 ml lysis buffer *A* (50 m*M* Tris pH 8.5, 300 m*M* NaCl). The cells were lysed using a FastPrep-24 (MPbio) with Lysing Matrix B (average size 74–150 µm) after the addition of DNAse I (deoxyribonuclease I from bovine pancreas; Sigma–Aldrich) for four cycles of 1 min in a 50 ml Falcon tube. The lysate was transferred to SS34 tubes for further centrifugation at 20 000 rev min^{-1} (JA-25.50 rotor, Beckman Coulter Avanti J-E) for 20 min. The supernatant was filtered using a syringe filter (0.22 µm, Millipore) and then loaded onto a 5 ml HisTrap column (GE Healthcare) charged with nickel and subsequently equilibrated with buffer *A*. After sample application, the column was washed with two column volumes of buffer *A* and two column volumes of washing buffer (50 m*M* Tris pH 8.5, 300 m*M* NaCl, 20 m*M* imidazole). The bound protein was eluted with 15 ml elution buffer (50 m*M* Tris pH 8.5, 300 m*M* NaCl, 250 m*M* imidazole). The eluted protein was concentrated to a volume of 5 ml and subjected to size-exclusion chromatography using a Superdex S75 16/60 column mounted on an ÄKTAxpress system (GE Healthcare) equilibrated in 25 m*M* HEPES pH 7.5, 150 m*M* NaCl, where it eluted as a single peak. The final sample purity was estimated to be 95% based on SDS–PAGE analysis (Supplementary Fig. S1*a*).

2.2. Analytical size-exclusion chromatography

Analytical size-exclusion chromatography was performed on an ÄKTA pure system (GE Healthcare) using a Superdex 200 Increase 3.2/300 column equilibrated in 25 m*M* HEPES pH 7.5, 150 m*M* NaCl. Column calibration was performed using albumin (molecular mass 66 kDa) and carbonic anhydrase (molecular mass 29 kDa) standards.

2.3. Measurement of dissociation constants

Affinity assays were conducted using a MicroCal iTC200 system (GE Healthcare) at 298 K using DPV022ΔC24 in

Table 1
Crystallographic data-collection and refinement statistics.

Values in parentheses are for the highest resolution shell.

	Native DPV022–Bim BH3	NaI-derivatized DPV022–Bim BH3	DPV022–Bak BH3	DPV022–Bax BH3
Data collection				
Space group	$P4_12_12$	$P4_12_12$	$P4_12_12$	$P4_12_12$
Unit-cell parameters				
a (Å)	94.39	94.42	93.26	92.48
b (Å)	94.39	94.42	93.26	92.48
c (Å)	45.54	45.46	45.62	45.53
$\alpha = \beta = \gamma$ (°)	90	90	90	90
Wavelength (Å)	0.9537	1.5498	0.9537	0.9537
Resolution (Å)	94.39–2.70 (2.78–2.70)	47.21–3.30 (3.57–3.30)	41.71–2.30 (2.39–2.30)	92.48–3.00 (3.18–3.00)
R_{sym} or R_{merge}†	0.078 (0.894)	0.131 (0.465)	0.100 (0.584)	0.140 (1.096)
$\langle I/\sigma(I)\rangle$	19.5 (2.8)	22.2 (8.7)	10.9 (3.1)	10.2 (1.7)
$CC_{1/2}$	0.999 (0.999)		0.996 (0.997)	0.998 (0.999)
Completeness (%)	100.0 (100.0)	100.0 (100.0)	97.7 (99.0)	100.0 (100.0)
Multiplicity	10.0 (10.3)	17.5 (18.3)	5.7 (5.8)	6.9 (7.2)
No. of reflections	6039 (771)	3394 (666)	9129 (953)	4297 (673)
No. of observed reflections	60365 (8090)	59512 (12169)	51582 (5518)	29816 (4860)
FOM (before/after density modification)		0.2/0.4		
Refinement				
Resolution range (Å)	19.99–2.70		41.71–2.30	43.24–3.00
Reflections (working set/test set)	5712/274		8664/446	4073/195
Protein atoms	1271		1277	1260
Solvent molecules	7 H_2O		42 H_2O/1 SO_4^{2-}	0
R_{work}/R_{free}‡	0.205/0.221		0.178/0.206	0.214/0.274
R.m.s.d., angles (°)	0.567		0.732	0.403
R.m.s.d., bonds (Å)	0.003		0.004	0.002
Ramachandran plot§ (%)				
Most favoured	98.0		97.4	94.0
Additionally allowed	2.0		2.6	6.0
Generously allowed	0		0	0
Disallowed	0		0	0

† $R_{merge} = \sum_{hkl}\sum_i |I_i(hkl) - \langle I(hkl)\rangle| / \sum_{hkl}\sum_i I_i(hkl)$, where $I_i(hkl)$ is the intensity of reflection hkl, $\sum_{hkl}$ is the sum over all reflections and $\sum_i$ is the sum over i measurements of reflection hkl. ‡ $R = \sum_{hkl} ||F_{obs}| - |F_{calc}|| / \sum_{hkl} |F_{obs}|$, where F_{obs} and F_{calc} are the observed and calculated structure-factor amplitudes, respectively. R_{work} and R_{free} were calculated using the working set and the test set, respectively. § Lovell *et al.* (2003).

25 m*M* HEPES pH 7.5, 150 m*M* NaCl at a final concentration of 20 µ*M*. Ligands at a concentration of 200 µ*M* were titrated using 19 injections of 2.0 µl of ligand. All affinity measurements were performed in triplicate. Protein concentrations were measured using a Nanodrop UV spectrophotometer (Thermo Scientific) at a wavelength of 280 nm. Peptide concentrations were calculated based on the dry peptide weight after synthesis. The BH3-domain peptides used were commercially synthesized using liquid-phase peptide synthesis (GenScript) and were purified to a final purity of 95%, and comprised the following sequences: hsBim (UniProt ID O43521-3; 51-DMRPEIWIAQELRRIGDEFNAYYARR-76), hsBak (UniProt ID Q16611-1; 67-PSSTMGQVGRQLAIIGDDINRRYDSE-92), hsBax (UniProt ID Q07812-1; 50-VPQDASTKKLSECLKRIGDELDSNMELQ-77), hsPuma (UniProt ID Q9BXH1-1; 130-EEQWAREIGAQLRRMADDLNAQYERR-155), hsNoxa (UniProt ID Q13794-1; 18-PAELEVECATQLRRFGDKLNFRQKLL-43), hsBad (UniProt ID Q92934-1; 103-NLWAAQRYGRELRRMSDEFVDSFKKG-128), hsBid (UniProt ID P55957-1; 79-SESQEDIIRNIARHLAQVGDSMDRSIPPGLVNGL-104), hsBik (UniProt ID Q13323-1; 51-MEGSDALALRLACIGDEMDVSLRAP-75), hsBeclin (UniProt ID Q14457-1; 107-GTMENLSRRLKVTGDLFDIMSGQT-130), hsHrk (UniProt ID O00198-1; 26-RSSAAQLTAARLKAIGDELHQRTMWR-51) and hsBmf (UniProt ID Q96LC9-1; 125-QHQAEVQIARKLQCIADQFHRLHVQQ-151)

2.4. Crystallization and data collection

The complexes of DPV022ΔC24 with Bim BH3, Bax BH3 and Bak BH3 were reconstituted by adding BH3-domain peptides at a 1:1.25 molar excess. The reconstituted complexes were concentrated to 5 mg ml^{-1} using centrifugal concentrators (Millipore), flash-cooled and stored under liquid nitrogen. High-throughput screening was carried out using 96-well sitting-drop trays (Swissci) and the vapour-diffusion method at 293 K at the CSIRO Collaborative Crystallization Centre, Melbourne, Australia. 150 nl protein was dispensed using a Crystal Mosquito robot (TTP Labtech) and 150 nl of the various reservoir solutions was dispensed using a Phoenix robot (Art Robbins). The initial crystallization conditions used were from commercially available screening kits (Crystal Screen and Crystal Screen 2 from Hampton Research and The PACT Suite from Qiagen). Hit optimization was performed in 24-well hanging-drop plates (EasyXtal DG-Tool, Qiagen) using 1 µl protein solution at a concentration of 5.0 mg ml^{-1} and 1 µl reservoir solution (total drop volume 2 µl). Hanging drops were placed over 0.4 ml reservoir solution for vapour diffusion at 293 K.

Crystals of DPV022ΔC24–Bim BH3 as well as those of DPV022ΔC24–Bak BH3 were obtained at 5 mg ml^{-1} using the sitting-drop method at 293 K in 17%(*w*/*v*) polyethylene glycol 8000, 0.2 *M* ammonium sulfate, 0.2 *M* MES buffer pH 5.5 (Supplementary Fig. S1*b*). DPV022ΔC24–Bax BH3 crystals grew in 20% polyethylene glycol 6000, 0.2 *M* ammonium sulfate, 0.2 *M* MES buffer pH 6.0. All three complexes formed needle-shaped crystals belonging to space group $P4_12_12$ in the tetragonal crystal system.

Crystals of DPV022ΔC24–Bim BH3 contained one chain of DPV022 and one chain of Bim, with a solvent content of 40.7%. The crystals were flash-cooled at 100 K in mother liquor supplemented with 25%(*v*/*v*) glycerol. All diffraction data were collected on the MX2 beamline at the Australian Synchrotron using a ADSC Quantum 315r CCD detector (Area Detector Systems Corporation, Poway, California, USA) with an oscillation range of 1.0° per frame. All native data were collected using a wavelength of 0.9537 Å.

A heavy-atom derivative was obtained by soaking crystals in mother liquor supplemented with 1 *M* NaI and 25%(*v*/*v*) glycerol for 60 s prior to flash-cooling at 100 K. Derivative data were collected using a wavelength of 1.549 Å. Diffraction data were integrated using *XDS* (Kabsch, 2010) and scaled using *AIMLESS* (Evans, 2006; Winn *et al.*, 2011). The structure was phased using single isomorphous replacement with anomalous scattering (SIRAS) using iodine ions. 15 sites were located using *SHELX* (Sheldrick, 2008, 2010) and phased using *AutoSol* in *PHENIX* (Terwilliger *et al.*, 2009; Adams *et al.*, 2010). Phasing in the resolution range 3.3–47.2 Å gave a figure of merit of 0.4. The DPV022ΔC24–Bim BH3 complex was built using *Coot* (Emsley & Cowtan, 2004) and refined using *PHENIX* (Afonine *et al.*, 2012).

The crystals of DPV022ΔC24–Bak BH3 and DPV022ΔC24–Bax BH3 had solvent contents of 39.4 and 38.2%, respectively, and were solved by molecular replacement with *Phaser* (McCoy *et al.*, 2007) using the previously determined structure of DPV022–BimBH3 as a search model. Diffraction data were integrated using *iMosflm* (Battye *et al.*, 2011) and scaled using *AIMLESS* (Evans, 2006; Winn *et al.*, 2011). The structures were built using *Coot* and refined using *PHENIX*. Details of the data-collection and refinement statistics are summarized in Table 1. All coordinate files have been deposited in the Protein Data

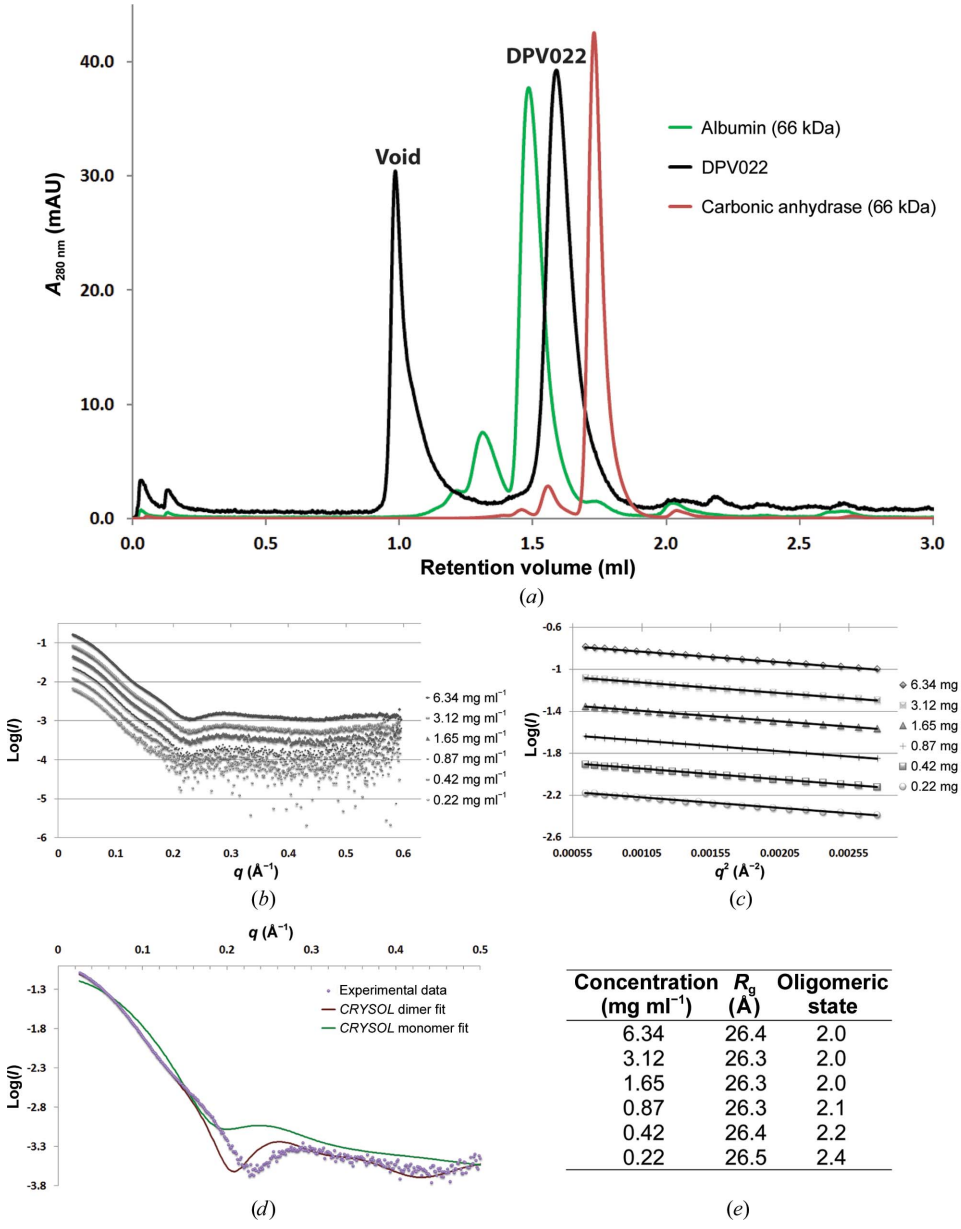

Concentration (mg ml^{-1})	R_g (Å)	Oligomeric state
6.34	26.4	2.0
3.12	26.3	2.0
1.65	26.3	2.0
0.87	26.3	2.1
0.42	26.4	2.2
0.22	26.5	2.4

(e)

Figure 1
DPV022ΔC24 appears to be a dimer in solution. (*a*) Size-exclusion chromatography of DPV022ΔC24 using a Superdex 200 Increase 3.2/300 column. The elution volume of the peak of interest (DPV022) is 1.56 ml. The molecular-weight standards shown are 66 kDa (albumin, green curve) and 29 kDa (carbonic anhydrase, red curve). (*b*) Log plot of DPV022ΔC24 raw SAXS data. Concentrations are in descending order commencing at 6.34 mg ml^{-1} (top), followed by 3.12, 1.65, 0.87, 0.42 and 0.22 mg ml^{-1}. (*c*) Guinier plots of DPV022ΔC24 SAXS data. Concentrations are, from top to bottom, 6.34, 3.12, 1.65, 0.87, 0.42 and 0.22 mg ml^{-1}. (*d*) *CRYSOL* analysis of SAXS data using monomeric and dimeric DPV022. (*e*) Summary of the SAXS data and analysis of the oligomeric state of DPV022ΔC24 in solution.

Bank under accession codes 4uf1, 4uf2 and 4uf3. All images were generated using *PyMOL* (DeLano, 2002).

2.5. Small-angle X-ray scattering

SAXS data were collected on the SAXS/WAXS beamline at the Australian Synchrotron. DPV022ΔC24 at concentrations of 0.22, 0.42, 0.87, 1.65, 3.12 and 6.34 mg ml^{-1} in 25 m*M* HEPES pH 7.5, 150 m*M* NaCl was measured in a q range between 0.025 and 0.6 Å^{-1} at 12 keV with a 1.6 m camera length at 293 K. The extinction coefficient for DPV022ΔC24 was 17 545 M^{-1} cm^{-1}. Normalization was achieved *via* an integrating beam stop. Data were measured on a Pilatus 1M detector (Dectris) and were absolute-scaled using distilled water. To control for radiation damage, the samples were measured in a 1.5 mm quartz capillary and flowed past the beam while 30 × 1 s exposures were measured on samples and blanks. Solvent blanks were obtained using the column flow-through from size-exclusion chromatography. The scattering images were integrated, averaged and calibrated against water using software specific to the beamline (Kirby & Cowieson, 2014). The radius of gyration (R_g) and the forward scattering $I(0)$ were determined by the Guinier approximation (Konarev *et al.*, 2003; Petoukhov *et al.*, 2012). Sample monodispersity was independently assessed using size-exclusion chromatography. *CRYSOL* analyses were performed using monomeric and dimeric structures of DPV022 (Svergun *et al.*, 1995). Details of the data collection are summarized in Table 2.

Table 2
Small-angle X-ray scattering data-collection and scattering-derived parameters.

Data-collection parameters	
Instrument	SAXS/WAXS beamline, Australian Synchrotron
Beam geometry (µm)	80 × 200
Wavelength (keV)	12
q range (Å^{-1})	0.025–0.600
Exposure time (s)	1 (per frame; 30 frames)
Concentration range (mg ml^{-1})	0.22–6.34
Temperature (K)	293
Structural parameters†	
$I(0)$ (from Guinier) (cm^{-1})	0.188 ± 0.000
R_g (from Guinier) (Å)	26.40 ± 0.02
Molecular-mass determination†	
Partial specific volume‡ (cm^3 g^{-1})	0.735
Contrast‡ ($\Delta\rho \times 10^{10}$ cm^{-2})	2.930
Molecular mass M_r [from $I(0)$] (Da)	38494
Calculated monomeric M_r from sequence (Da)	19606
Software employed	
Primary data reduction	SAXS/WAXS beamline software
Data processing	*PRIMUS*

† Reported for 6.34 mg ml^{-1}. ‡ Determined with *MULCh* (Whitten *et al.*, 2008).

3. Results

3.1. DPV022 is a dimeric protein in solution

A construct spanning residues 1–155 of DPV022 was expressed using *E. coli* and purified using a two-step purification strategy (Fig. 1*a*, Supplementary Fig. S1*a*). During size-exclusion chromatography DPV022 eluted at a volume commensurate with a dimeric configuration (Fig. 1*a*) with a predicted molecular weight of 43.7 kDa. To confirm the oligomeric state of DPV022, we performed small-angle X-ray scattering (SAXS; Table 2) using six concentrations ranging from 6.34 to 0.22 mg ml^{-1}. The scattering-curve profile was conserved throughout the concentration range tested (Fig. 1*b*). A straight line was achieved in the low-q region in a Guinier plot (Fig. 1*c*) and the determined radius of gyration was not significantly concentration-dependent, suggesting an absence of concentration effects. The molecular mass calculated from $I(0)$ on the absolute scattering scale across the concentration range was ∼41.3 kDa, corresponding to an oligomerization state of ∼2 (Fig. 1*e*). *CRYSOL* analysis was performed using monomeric and dimeric DPV022 structures (Fig. 1*d*; Svergun *et al.*, 1995) and, as expected, the DPV022 monomer presents a completely different scattering profile and a smaller size incompatible with our experimental data. The DPV022 dimer structure shows a similar scattering profile to that obtained experimentally, with some minor variations that could result from inherent protein flexibility in solution compared with the crystalline state of the fitted structure.

3.2. DPV022 displays a highly restricted BH3-domain ligand-binding profile

The interplay between anti-apoptotic Bcl-2 proteins and their death-inducing counterparts, the BH3-only proteins and the multi-domain Bak and Bax, ultimately determines whether a cell lives or dies. To understand the molecular basis for DPV022-mediated inhibition of apoptosis, we assessed the binding of various BH3-domain peptides from human BH3-only proteins as well as BH3 domains from the pro-apoptotic proteins Bak and Bax (Fig. 2). Unexpectedly, DPV022 only revealed modest affinity for the BH3 domain of Bim with a K_d of 340 n*M* (Figs. 2*a* and 2*e*), and only displayed weak affinity for Bax and Bak BH3 domains at 4040 n*M* (Figs. 2*b* and 2*e*) and 6980 n*M* (Figs. 2*c* and 2*e*), respectively. No other assessed BH3-domain peptide showed detectable binding (Figs. 2*d* and 2*e*).

3.3. Crystal structures of DPV022 in complex with Bim, Bax and Bak BH3 domains

To obtain insight into the structural basis of DPV022-mediated inhibition of apoptosis, we determined the crystal structures of DPV022 in complex with all identified pro-death ligands: Bim, Bax and Bak BH3 domains. Despite a lack of detectable sequence identity with cellular Bcl-2 proteins, DPV022 adopts a Bcl-2-like fold comprising eight α-helices (Fig. 3*a*). In accord with our size-exclusion chromatography and SAXS analysis, DPV022 adopts a dimeric configuration in which the α1 helices of two neighbouring chains are arranged in a domain swap. Dimerization appears to be the consequence of a shortened loop connecting the α1 and α2 helices, comprising only two amino acids (Leu31 and Asn32), and thus preventing the typically observed monomeric topology. This arrangement is near-identical (r.m.s.d of 2.1 Å over 129 C^α atoms) to that found in *Vaccinia virus* F1L (Fig. 3*b*; Kvansakul *et al.*, 2008; Campbell *et al.*, 2014) despite the limited sequence

identity (23% over the Bcl-2 fold; Fig. 4). Dimeric DPV022 harbours two canonical Bcl-2 binding grooves which are capable of engaging BH3-domain ligands.

3.4. BH3-domain binding of DPV022

The two ligand-binding grooves in DPV022 are formed by α-helices 2–5, with helices 2–4 providing the walls of the groove and helix 5 providing the floor (Fig. 3*c*). The Bim, Bax and Bak BH3 domains are bound with an identical topology, in which key hydrophobic residues from the BH3 domain protrude into four hydrophobic pockets in the ligand-binding groove (Figs. 5*a*, 5*c* and 5*d*). The ligand-binding groove is unexpectedly smaller compared with other viral or cellular Bcl-2 molecules (Fig. 5*b*) owing to the positioning of Gln63 and Lys77 (Fig. 3*c*), the side chains of which block the end of the binding groove close to the α3–α4 turn. This obstacle forces the N-termini of the bound BH3 domains to move out of the binding groove.

In the DPV022–Bim BH3 complex the hydrophobic residues Ile58, Leu62, Ile65 and Phe69 are accommodated in four hydrophobic pockets (Fig. 5*a*). In addition, several hydrogen and ionic bonds are formed, including those between $Tyr53^{DPV}$ and $Glu68^{Bim}$ (charged hydrogen bond, 3.37 Å) and between $Asp85^{DPV}$ and $Arg63^{Bim}$ (salt bridge, 2.66 Å), as well as between $Arg87^{DPV}$ and $Asp67^{Bim}$ (salt bridge, 2.45 Å).

In the DPV022ΔC24–Bak BH3 complex (Fig. 5*c*), the Bak BH3 hydrophobic residues Val74, Leu78, Ile81 and Ile85 protrude into the ligand-binding groove. In contrast to the complex with Bim BH3, only one salt bridge is formed

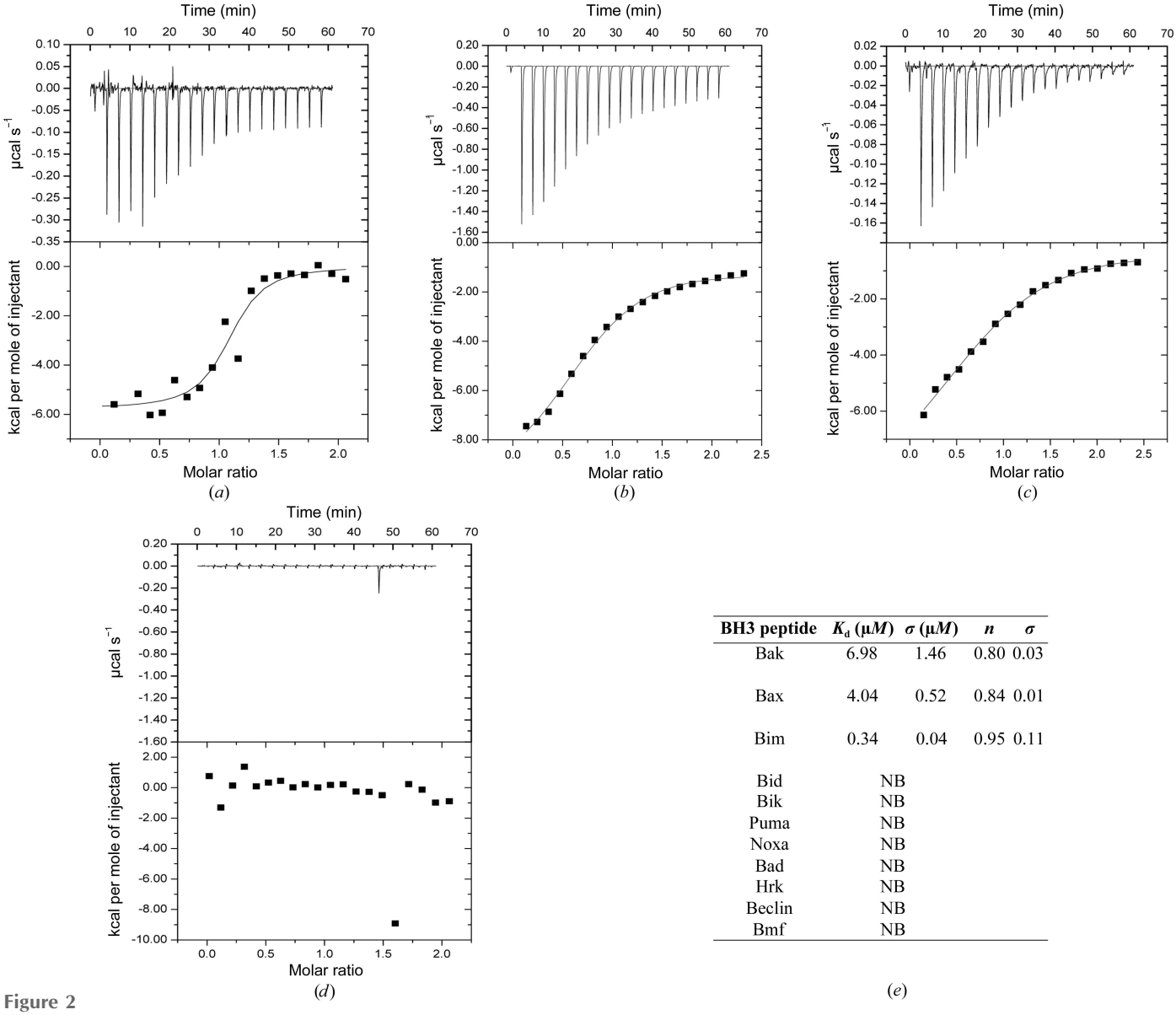

BH3 peptide	K_d (µ*M*)	σ (µ*M*)	*n*	σ
Bak	6.98	1.46	0.80	0.03
Bax	4.04	0.52	0.84	0.01
Bim	0.34	0.04	0.95	0.11
Bid	NB			
Bik	NB			
Puma	NB			
Noxa	NB			
Bad	NB			
Hrk	NB			
Beclin	NB			
Bmf	NB			

(e)

Figure 2
DPV022 interacts with three BH3 domains of pro-apoptotic proteins. Raw heats measured by isothermal titration calorimetry of DPV022ΔC24 with BH3-domain peptides of human pro-apoptotic Bcl-2 proteins. (*a*) DPV022ΔC24 with Bim BH3. (*b*) DPV022ΔC24 with Bax BH3. (*c*) DPV022ΔC24 with Bak BH3. (*d*) DPV022ΔC24 with Puma BH3. (*e*) Table of binding constants (K_d) obtained by fitting ITC data to a single-state binding model. NB denotes no binding; σ is the standard deviation calculated from triplicate experiments.

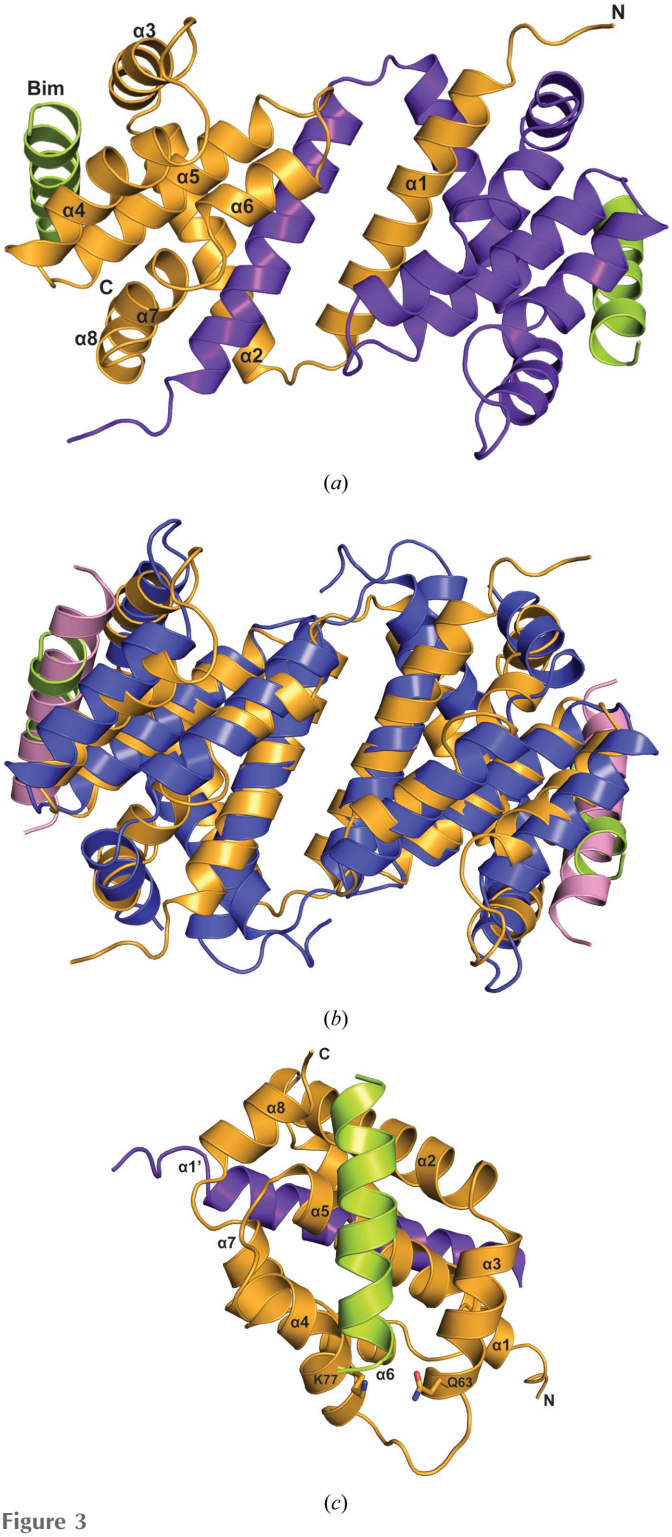

Figure 3
The DPV022–Bim BH3 crystal structure reveals a dimeric configuration formed *via* a domain swap harbouring two independent ligand-binding sites. (*a*) Cartoon representation of DPV022 (gold and purple) bound to Bim BH3 (green). The view is down the twofold-symmetry axis between the domain-swapped α1 helices. (*b*) Superimposition of DPV022–Bim BH3 (DPV022 is shown in gold and Bim is shown in green) with modified *Vaccinia virus* Ankara (MVA) F1L–Bim BH3 (F1L is shown in blue and Bim is shown in magenta), the closest known poxviral Bcl-2 structure (PDB entry 2vty). (*c*) Cartoon representation of DPV022 (gold and purple) bound to Bim BH3 (green). This view is into the hydrophobic binding groove formed by helices α2–α5.

between Bak BH3 and DPV022 (between $Arg87^{DPV}$ and $Asp83^{Bak}$, 2.66 Å). An additional hydrogen bond is formed between $Ser59^{DPV}$ and $Gln77^{Bak}$ (hydrogen bond, 3.27 Å).

In the DPV022–Bax BH3 complex (Fig. 5*d*), the hydrophobic residues Leu59, Leu63, Ile66 and Leu70 are accommodated in four hydrophobic pockets. Here, two salt bridges are formed between $Arg87^{DPV}$ and $Asp68^{Bax}$ (2.3 Å) as well as between $Asp56^{DPV}$ and $Arg65^{Bax}$ (3.5 Å). Two additional hydrogen bonds are formed between $Ser89^{DPV}$ and $Asp71^{Bax}$ (charged hydrogen bond, 2.8 Å) and between $Glu80^{DPV}$ and $Ser60^{Bax}$ (charged hydrogen bond, 2.7 Å).

4. Discussion

Inhibition of premature host-cell apoptosis is an important step during viral infection, and viruses utilize an impressive array of molecules to counter initial apoptotic defences by their hosts (Galluzzi *et al.*, 2008; Best, 2008). Viral Bcl-2 proteins have been shown to be crucial virulence factors that disarm apoptotic defences. Many viruses encode Bcl-2 homologues that are readily identifiable at the sequence level, including adenovirus E1B19K (White *et al.*, 1992), KSHV KsBcl-2 (Cheng *et al.*, 1997), EBV BHRF-1 (Henderson *et al.*, 1993), γ-herpesvirus 68 M11 (Wang *et al.*, 1999) and *African swine fever virus* A179L (Brun *et al.*, 1996). Similarly, amongst the poxviruses Bcl-2 homologues have been identified in *Fowlpox virus* (FPV039; Banadyga *et al.*, 2009) and *Canarypox virus* (CPV058; Tulman *et al.*, 2004). However, particularly amongst the poxviruses, several inhibitors of apoptosis were identified that did not harbour detectable sequence identity to cellular Bcl-2 proteins (Kvansakul *et al.*, 2007, 2008; Okamoto *et al.*, 2012); however, structure determination revealed that *Myxoma virus* M11L (Kvansakul *et al.*, 2007; Douglas *et al.*, 2007) and *Vaccinia virus* F1L (Kvansakul *et al.*, 2008) both adopt Bcl-2 folds.

We recently identified DPV022 as a putative viral Bcl-2 (vBcl-2) protein (Banadyga *et al.*, 2011). Despite lacking obvious sequence identity to cellular Bcl-2 proteins, DPV022 was shown to engage Bak and Bax, and potently protects against apoptosis in cellular assays. To define the molecular basis of DPV022-mediated inhibition of apoptosis, we systematically evaluated the ability of DPV022 to bind to peptides spanning the BH3 domain of death-inducing Bcl-2 family members. DPV022 only displayed moderate affinities for Bim (340 n*M*), Bax (4040 n*M*) and Bak (6980 n*M*), and did not bind to any other pro-death Bcl-2 protein. However, despite only modest affinities for Bim, Bax and Bak, it has previously been shown that DPV022 is a potent inhibitor of apoptosis; clearly, the modest affinities in our peptide-based assays are not a hindrance to high levels of protection against apoptosis in the cellular context (Banadyga *et al.*, 2011). This behaviour bears a striking resemblance to *Vaccinia virus* F1L, which was the first domain-swapped dimeric vBcl-2 to be identified and also binds exclusively to Bim, Bax and Bak with modest affinities (Kvansakul *et al.*, 2008).

We then determined the crystal structures of DPV022 in complex with all identified binding partners. Despite lacking

detectable sequence identity to cellular Bcl-2 proteins, DPV022 adopts a Bcl-2 fold harbouring the canonical ligand-binding groove found in all other anti-apoptotic members of this family. Examination of the interactions between Bim, Bax and Bak and the ligand-binding groove of DPV022 reveal that the positioning of Gln63 and Lys77 on the α3 and α4 helices shortens the binding groove, thus forcing the N-termini of bound BH3 domains to move out of the binding groove. This obstruction is likely to be a contributing factor to the modest affinities for BH3-domain ligands that we observed in calorimetric assays. Further examination of the detailed DPV022–ligand interactions reveals that DPV022 unexpectedly utilizes multiple ionic interactions that mimic the binding of BH3 domains to cellular anti-apoptotic Bcl-2 members. This is in marked contrast to *Vaccinia virus* F1L, which does not rely on ionic interactions to engage BH3-domain ligands (Campbell *et al.*, 2014). In the DPV022–Bim BH3 complex, two salt bridges between Asp85^{DPV} and Arg63^{Bim} and between Arg87^{DPV} and Asp67^{Bim} are observed. These ionic interactions are characteristic of cellular Bcl-2 or obvious vBcl-2 complexes with BH3 domains, with the hallmark interaction being between the arginine from the conserved NWG**R** sequence in the BH1 motif (Kvansakul & Hinds, 2013*b*) and an aspartic acid on the bound BH3 domain (Petros *et al.*, 2004). Similarly, the DPV022–Bax BH3 complex also features two ionic interactions with the BH3 domain: Asp56^{DPV}–Arg65^{Bax} and Arg87^{DPV}–Asp68^{Bax}. In contrast, the DPV022–Bak BH3 complex only features a single ionic interaction, Arg87^{DPV}–Asp83^{Bak}. Interestingly, a comparison with protein–ligand interactions in cellular Bcl-2 complexes reveals that A1 in complex with Bim (Herman *et al.*, 2008; 19% sequence identity to DPV022 over the Bcl-2 fold; Fig. 4) displays striking similarities to DPV022 in the manner in which A1 binds the BH3-domain peptide. A1 features a double salt bridge between Asp81^{A1} and Arg63^{Bim} and between Arg88^{A1} and Asp67^{Bim}, with the arginine from the NWG**R** motif, as well as a third salt bridge involving Glu47^{A1} and Arg62^{Bim} (Fig. S2*a*; Herman *et al.*, 2008).

A comparison of *Vaccinia virus* F1L and *Deerpox virus* DPV022, which both adopt domain-swapped topologies, with other Bcl-2 proteins that are monomeric reveals that a short loop connecting the α1 and α2 helices is likely to be at least a contributing factor to the domain swap. Mammalian Bcl-2 proteins that are monomeric have longer α1–α2 loops, including A1 (12 residues) and Mcl-1 (17 residues) as well as Bcl-2 (68 residues) and Bcl-x$_L$ (64 residues). In contrast, the corresponding loops in F1L and DPV022 are two residues in length. Notably, truncation of the Bcl-x$_L$ loop to six residues forced the adoption of a domain-swapped topology (Oberstein *et al.*, 2007). However, the α1–α2 loop length is unlikely to be the sole determinant with respect to domain swapping. In M11L the α1–α2 loop is only eight residues in length, yet M11L is monomeric. Inspection of the α1 helix in M11L indicates that it is relatively short (11 residues) compared with Bcl-x$_L$ (19 residues). It appears likely that a short α1 helix can still lead to a monomeric Bcl-2 topology even in the presence of a comparatively short connecting loop (as is the case with M11L), whereas longer α1 helices such as in Bcl-x$_L$ necessitate a longer α1–α2 loop to adopt a monomeric topology.

Our identification of other domain-swapped dimeric vBcl-2 proteins that only display modest affinities for their death-inducing ligands suggests the existence of (at least) three discrete classes of vBcl-2 proteins. Class 1 vBcl-2 proteins comprise those members that are monomeric and engage death-inducing Bcl-2 ligands with high nanomolar affinities. This class includes the obvious anti-apoptotic vBcl-2 proteins such as BHRF1 (Kvansakul *et al.*, 2010) and KsBcl-2 (Flanagan & Letai,

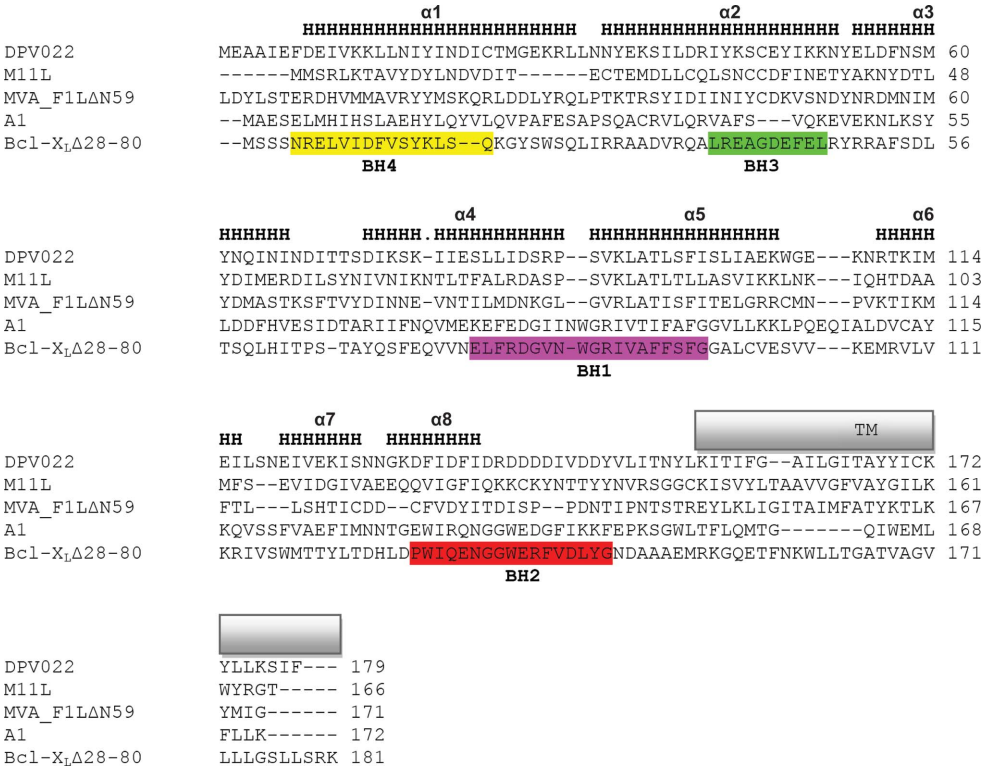

Figure 4
Sequence and structural alignment of DPV022 with the two closest related poxviral Bcl-2 proteins M11L and MVA F1L as well as two cellular Bcl-2 proteins, A1 and Bcl-x$_L$. Sequence and structural alignment of DPV022 with M11L, MVA F1L, A1 and Bcl-x$_L$. The marked secondary-structure elements (shown as H) are based on DPV022. The putative transmembrane domains (TM) are boxed. The different Bcl-2 homology motifs are colour-coded.

2007), as well as M11L (Kvansakul *et al.*, 2007) and M11 (Ku *et al.*, 2008) (Table 3). In contrast, class 2 vBcl-2 proteins comprise *Vaccinia virus* F1L (Kvansakul *et al.*, 2008), *Variola virus* F1L (Marshall *et al.*, 2014) and DPV022. Class 2 proteins

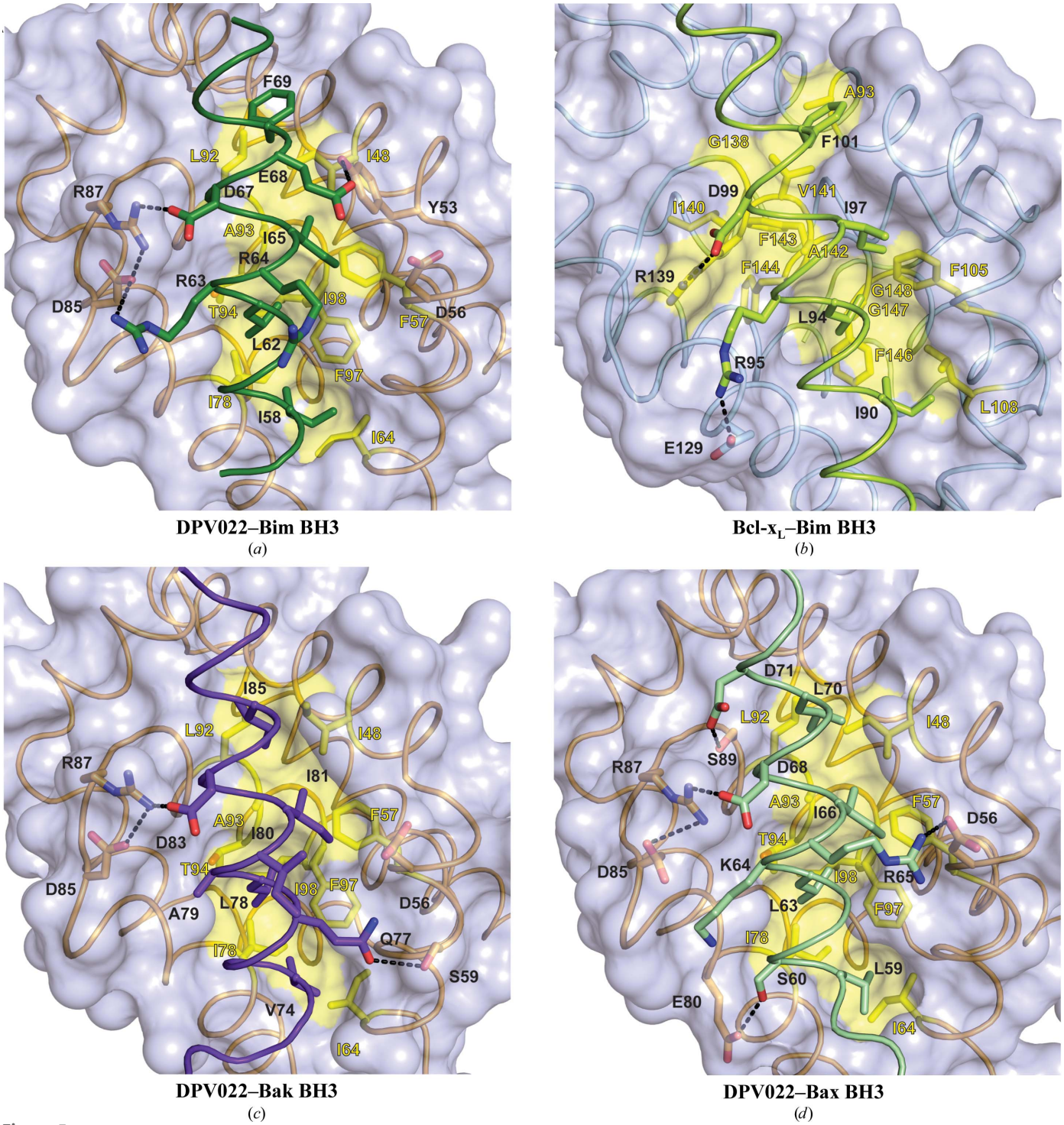

Figure 5
Detailed views of the interactions between DPV022 and pro-apoptotic BH3 domains. (*a*) Surface diagram of the binding interface formed by the DPV022–Bim BH3 complex. The DPV022 surface is shown in grey. DPV022 and Bim BH3 residues are labelled in black, except for the residues involved in the hydrophobic surface, which are labelled in yellow. (*b*) Surface diagram of the binding interface formed by the Bcl-x$_L$–Bim complex (PDB entry 1pq1). The Bcl-x$_L$ surface is shown in grey. Bcl-x$_L$ and Bim BH3 residues are labelled in black, except for the residues involved in the hydrophobic surface, which are labelled in yellow. (*c*) Surface diagram of the binding interface formed by the DPV022–Bax BH3 complex. DPV022 and Bak BH3 residues are coloured black, except for the residues involved in the hydrophobic surface, which are labelled in yellow. (*d*) Surface diagram of the binding interface formed by the DPV022–Bax complex. DPV022 and Bak BH3 residues are coloured black, except for the residues involved in the hydrophobic surface, which are labelled in yellow.

Table 3
Binding affinities of known pro-survival Bcl-2 proteins to BH3-domain ligands.

NB, no binding.

	Poxviral Bcl-2							Herpesviral Bcl-2			Cellular Bcl-2			
	SPPV14†	M11L†	MVA F1L†	VAR F1L‡	DPV022‡	N1L§	BHRF1‡	KsBcl-2§	M11‡	Bcl-2†	Bcl-w†	Bcl-x_L†	Mcl-1†	A1‡
Bad	>2000	>1000	NB	NB	NB	>1000	>2000	>1000	n/a	16	30	5.3	>100000	15000
Bid	341	100	NB	3220	NB	152	109	112	232	6800	40	82	2100	1
Bik	>2000	>1000	NB	NB	NB	n/a	>2000	>1000	n/a	850	12	43	1700	58
Bim	26	5	250	NB	340	72	18	29	131	2.6	4.3	4.6	2.4	1
Bmf	67	100	NB	NB	NB	n/a	>2000	>1000	300	3	9.8	9.7	1100	180
Hrk	63	>1000	NB	NB	NB	n/a	>1000	>1000	719	320	49	3.7	370	46
Noxa	>2000	>1000	NB	NB	NB	n/a	>2000	>1000	132	>100000	>100000	>100000	24	20
Puma	65	>1000	NB	NB	NB	n/a	70	69	370	3.3	5.1	6.3	5	1
Beclin	n/a	n/a	n/a	NB	NB	n/a	n/a	n/a	40.2	n/a	n/a	2300	n/a	n/a
Bak	46	50	4300	2640	6930	71	150	<50	76.3	>1000	500	50	10	3
Bax	32	75	1850	960	4040	n/a	1400	980	690	100	58	130	12	n/a

† Affinity measured in n*M* by SPR (K_d). ‡ Affinity measured in n*M* by isothermal calorimetry (K_d). § Affinity measured in n*M* by fluorescence polarization (IC_{50}).

are characterized by their domain-swapped dimeric topology and their characteristic ligand-binding profile, which is highly restricted and only features modest affinities for pro-death Bcl-2 members, typically in the low-nanomolar or micromolar range (Table 3). Class 3 vBcl-2 proteins comprise vBcl-2 proteins that do not bind pro-death Bcl-2 proteins and their BH3 domains; they instead harbour diverse immune-modulatory functions such as inhibition of the NF-κB pathway and IRF3. This class contains members with experimentally determined structures, including A49, A52, B14 and K7 (Neidel *et al.*, 2015; Graham *et al.*, 2008; Oda *et al.*, 2009), and is likely to be expanded once structures are available for several other predicted members (see, for example, González & Esteban, 2010).

Based on this classification there is no clear place for N1, which harbours both anti-apoptotic and NF-κB inhibitory activity (de Motes *et al.*, 2011). From a structural perspective one could assign N1 to class 3, since it is a cytosolic protein lacking a mitochondrial anchor sequence and forms dimers (Cooray *et al.*, 2007; Aoyagi *et al.*, 2007) in a manner reminiscent of B14 and A52 (Graham *et al.*, 2008). However, N1 also engages BH3-domain peptides from several pro-death Bcl-2 proteins with nanomolar affinities (Aoyagi *et al.*, 2007), which would favour placement in one of the other classes.

It remains to be determined whether DPV022 acts mechanistically in a similar manner to *Vaccinia virus* F1L. Although they share a striking similarity in ligand-binding behaviour, further studies in the context of a live viral infection are required to demonstrate whether DPV022 also acts primarily *via* Bim as does *Vaccinia virus* F1L (Campbell *et al.*, 2014). A curious feature of vBcl-2 proteins appears to be an inability to engage Noxa (Kvansakul & Hinds, 2013*a*). Whether or not this feature is of biological significance remains to be determined; however, the ability of *Vaccinia virus* F1L to replace Mcl-1 (Campbell *et al.*, 2010), a crucial Noxa binder (Day *et al.*, 2008), suggests that there may be more to the role of Noxa in the context of viral infections than we understand (Ferrer *et al.*, 2011).

Although the pro-death Bcl-2 ligand-binding profile of DPV022 is very similar to that of *Vaccinia virus* F1L, both in terms of the ligands that are bound as well as their affinities, it is likely that functionally significant differences exist in their ability to engage with host-cell signalling pathways. Unlike *Vaccinia virus* F1L, the DPV022 sequence is a noticeably shorter and lacks the distinct N-terminal repeat sequences and extensions that are a feature of F1L. Crucially, these additional ~60 residues in F1L have been shown to harbour both caspase-9 inhibitory function (Zhai *et al.*, 2010; Yu *et al.*, 2011) in a region spanning residues 1–15 as well as a pyroptosis inhibitory function suggested to reside within residues 32–37 (Gerlic *et al.*, 2013). It remains to be clarified how the different functions of F1L work together to modulate host-cell responses during viral infection, however in the case of DPV022 it seems unlikely that similar caspase-9 or pyroptosis inhibitory functionality is present since the signature N-terminal extension found in *Vaccinia virus* F1L is absent.

Viral Bcl-2 members have displayed considerably more diversity in their structural features as well as their range and mode of engagement of death-inducing cellular Bcl-2 proteins, compared with their anti-apoptotic host counterparts (Kvansakul & Hinds, 2013*a*). This is reinforced by our findings that DPV022 is a domain-swapped Bcl-2 protein harbouring a highly restricted BH3 domain-binding profile with only modest affinities for Bim, Bak and Bax.

Acknowledgements

We thank the staff at beamline MX2 and the SAXS/WAXS beamline at the Australian Synchrotron for help with X-ray data collection, and Janet Newman and Shane Seabrook at the CSIRO C3 Collaborative Crystallization Centre for assistance with crystallization. We thank Begona Heras, Nathan Cowieson and Grant Mills for helpful discussions.

References

Adams, J. M. & Cory, S. (1998). *Science*, **281**, 1322–1326.
Adams, P. D. *et al.* (2010). *Acta Cryst.* D**66**, 213–221.
Afonine, P. V., Grosse-Kunstleve, R. W., Echols, N., Headd, J. J., Moriarty, N. W., Mustyakimov, M., Terwilliger, T. C., Urzhumtsev, A., Zwart, P. H. & Adams, P. D. (2012). *Acta Cryst.* D**68**, 352–367.
Altmann, M. & Hammerschmidt, W. (2005). *PLoS Biol.* **3**, e404.

Aoyagi, M., Zhai, D., Jin, C., Aleshin, A. E., Stec, B., Reed, J. C. & Liddington, R. C. (2007). *Protein Sci.* **16**, 118–124.

Banadyga, L., Gerig, J., Stewart, T. & Barry, M. (2007). *J. Virol.* **81**, 11032–11045.

Banadyga, L., Lam, S.-C., Okamoto, T., Kvansakul, M., Huang, D. C. & Barry, M. (2011). *J. Virol.* **85**, 1922–1934.

Banadyga, L., Veugelers, K., Campbell, S. & Barry, M. (2009). *J. Virol.* **83**, 7085–7098.

Bartlett, N., Symons, J. A., Tscharke, D. C. & Smith, G. L. (2002). *J. Gen. Virol.* **83**, 1965–1976.

Battye, T. G. G., Kontogiannis, L., Johnson, O., Powell, H. R. & Leslie, A. G. W. (2011). *Acta Cryst.* D**67**, 271–281.

Best, S. M. (2008). *Annu. Rev. Microbiol.* **62**, 171–192.

Brun, A., Rivas, C., Esteban, M., Escribano, J. M. & Alonso, C. (1996). *Virology*, **225**, 227–230.

Campbell, S., Hazes, B., Kvansakul, M., Colman, P. & Barry, M. (2010). *J. Biol. Chem.* **285**, 4695–4708.

Campbell, S., Thibault, J., Mehta, N., Colman, P. M., Barry, M. & Kvansakul, M. (2014). *J. Virol.* **88**, 8667–8677.

Cheng, E. H.-Y., Nicholas, J., Bellows, D. S., Hayward, G. S., Guo, H.-G., Reitz, M. S. & Hardwick, J. M. (1997). *Proc. Natl Acad. Sci. USA*, **94**, 690–694.

Chipuk, J. E. & Green, D. R. (2008). *Trends Cell Biol.* **18**, 157–164.

Chipuk, J. E., Moldoveanu, T., Llambi, F., Parsons, M. J. & Green, D. R. (2010). *Mol. Cell*, **37**, 299–310.

Cooray, S., Bahar, M. W., Abrescia, N. G. A., McVey, C. E., Bartlett, N. W., Chen, R. A.-J., Stuart, D. I., Grimes, J. M. & Smith, G. L. (2007). *J. Gen. Virol.* **88**, 1656–1666.

Czabotar, P. E., Westphal, D., Dewson, G., Ma, S., Hockings, C., Fairlie, W. D., Lee, E. F., Yao, S., Robin, A. Y., Smith, B. J., Huang, D. C. S., Kluck, R. M., Adams, J. M. & Colman, P. M. (2013). *Cell*, **152**, 519–531.

Day, C. L., Smits, C., Fan, F. C., Lee, E. F., Fairlie, W. D. & Hinds, M. G. (2008). *J. Mol. Biol.* **380**, 958–971.

DeLano, W. L. (2002). *PyMOL*. http://www.pymol.org.

Douglas, A. E., Corbett, K. D., Berger, J. M., McFadden, G. & Handel, T. M. (2007). *Protein Sci.* **16**, 695–703.

Eitz Ferrer, P., Potthoff, S., Kirschnek, S., Gasteiger, G., Kastenmüller, W., Ludwig, H., Paschen, S. A., Villunger, A., Sutter, G., Drexler, I. & Häcker, G. (2011). *PLoS Pathog.* **7**, e1002083.

Emsley, P. & Cowtan, K. (2004). *Acta Cryst.* D**60**, 2126–2132.

Evans, P. (2006). *Acta Cryst.* D**62**, 72–82.

Fischer, S. F., Ludwig, H., Holzapfel, J., Kvansakul, M., Chen, L., Huang, D. C. S., Sutter, G., Knese, M. & Häcker, G. (2005). *Cell Death Differ.* **13**, 109–118.

Flanagan, A. & Letai, A. (2007). *Cell Death Differ.* **15**, 580–588.

Galluzzi, L., Brenner, C., Morselli, E., Touat, Z. & Kroemer, G. (2008). *PLoS Pathog.* **4**, e1000018.

Gerlic, M., Faustin, B., Postigo, A., Yu, E. C.-W., Proell, M., Gombosuren, N., Krajewska, M., Flynn, R., Croft, M., Way, M., Satterthwait, A., Liddington, R. C., Salek-Ardakani, S., Matsuzawa, S. & Reed, J. C. (2013). *Proc. Natl Acad. Sci. USA*, **110**, 7808–7813.

González, J. M. & Esteban, M. (2010). *Virol. J.* **7**, 59.

Graham, S. C., Bahar, M. W., Cooray, S., Chen, R. A.-J., Whalen, D. M., Abrescia, N. G. A., Alderton, D., Owens, R. J., Stuart, D. I., Smith, G. L. & Grimes, J. M. (2008). *PLoS Pathog.* **4**, e1000128.

Graham, K. A., Opgenorth, A., Upton, C. & McFadden, G. (1992). *Virology*, **191**, 112–124.

Green, D. R. & Kroemer, G. (2004). *Science*, **305**, 626–629.

Henderson, S., Huen, D., Rowe, M., Dawson, C., Johnson, G. & Rickinson, A. (1993). *Proc. Natl Acad. Sci. USA*, **90**, 8479–8483.

Herman, M. D., Nyman, T., Welin, M., Lehtiö, L., Flodin, S., Trésaugues, L., Kotenyova, T., Flores, A. & Nordlund, P. (2008). *FEBS Lett.* **582**, 3590–3594.

Kabsch, W. (2010). *Acta Cryst.* D**66**, 125–132.

Kirby, N. M. & Cowieson, N. P. (2014). *Curr. Opin. Struct. Biol.* **28**, 41–46.

Konarev, P. V., Volkov, V. V., Sokolova, A. V., Koch, M. H. J. & Svergun, D. I. (2003). *J. Appl. Cryst.* **36**, 1277–1282.

Ku, B., Woo, J.-S., Liang, C., Lee, K.-H., Hong, H.-S., Kim, K. S., Jung, J. U. & Oh, B.-H. (2008). *PLoS Pathog.* **4**, e25.

Kvansakul, M. & Hinds, M. G. (2013*a*). *Cell Death Dis.* **4**, e909.

Kvansakul, M. & Hinds, M. G. (2013*b*). *Methods Enzymol.* **544**, 49–74.

Kvansakul, M., van Delft, M. F., Lee, E. F., Gulbis, J. M., Fairlie, W. D., Huang, D. C. S. & Colman, P. M. (2007). *Mol. Cell*, **25**, 933–942.

Kvansakul, M., Wei, A. H., Fletcher, J. I., Willis, S. N., Chen, L., Roberts, A. W., Huang, D. C. S. & Colman, P. M. (2010). *PLoS Pathog.* **6**, e1001236.

Kvansakul, M., Yang, H., Fairlie, W., Czabotar, P., Fischer, S., Perugini, M., Huang, D. C. S. & Colman, P. (2008). *Cell Death Differ.* **15**, 1564–1571.

Lovell, S. C., Davis, I. W., Arendall, W. B., de Bakker, P. I., Word, J. M., Prisant, M. G., Richardson, J. S. & Richardson, D. C. (2003). *Proteins*, **50**, 437–450.

Maluquer de Motes, C., Cooray, S., Ren, H., Almeida, G. M., McGourty, K., Bahar, M. W., Stuart, D. I., Grimes, J. M., Graham, S. C. & Smith, G. L. (2011). *PLoS Pathog.* **7**, e1002430.

Marshall, B., Puthalakath, H., Caria, S., Chugh, S., Doerflinger, M., Colman, P. M. & Kvansakul, M. (2014). *Cell Death Dis.* **6**, e1680.

McCoy, A. J., Grosse-Kunstleve, R. W., Adams, P. D., Winn, M. D., Storoni, L. C. & Read, R. J. (2007). *J. Appl. Cryst.* **40**, 658–674.

Neidel, S., Maluquer de Motes, C., Mansur, D. S., Strnadova, P., Smith, G. L. & Graham, S. C. (2015). *J. Biol. Chem.* **290**, 5991–6002.

Oberstein, A., Jeffrey, P. D. & Shi, Y. (2007). *J. Biol. Chem.* **282**, 13123–13132.

Oda, S., Schröder, M. & Khan, A. R. (2009). *Structure*, **17**, 1528–1537.

Okamoto, T., Campbell, S., Mehta, N., Thibault, J., Colman, P. M., Barry, M., Huang, D. C. S. & Kvansakul, M. (2012). *J. Virol.* **86**, 11501–11511.

Petoukhov, M. V., Franke, D., Shkumatov, A. V., Tria, G., Kikhney, A. G., Gajda, M., Gorba, C., Mertens, H. D. T., Konarev, P. V. & Svergun, D. I. (2012). *J. Appl. Cryst.* **45**, 342–350.

Petros, A. M., Olejniczak, E. T. & Fesik, S. W. (2004). *Biochim. Biophys. Acta*, **1644**, 83–94.

Shamas-Din, A., Brahmbhatt, H., Leber, B. & Andrews, D. W. (2011). *Biochim. Biophys. Acta*, **1813**, 508–520.

Sheldrick, G. M. (2008). *Acta Cryst.* A**64**, 112–122.

Sheldrick, G. M. (2010). *Acta Cryst.* D**66**, 479–485.

Svergun, D., Barberato, C. & Koch, M. H. J. (1995). *J. Appl. Cryst.* **28**, 768–773.

Terwilliger, T. C., Adams, P. D., Read, R. J., McCoy, A. J., Moriarty, N. W., Grosse-Kunstleve, R. W., Afonine, P. V., Zwart, P. H. & Hung, L.-W. (2009). *Acta Cryst.* D**65**, 582–601.

Tulman, E., Afonso, C., Lu, Z., Zsak, L., Kutish, G. & Rock, D. (2004). *J. Virol.* **78**, 353–366.

Vaux, D. L., Cory, S. & Adams, J. M. (1988). *Nature (London)*, **335**, 440–442.

Wang, G.-H., Garvey, T. L. & Cohen, J. I. (1999). *J. Gen. Virol.* **80**, 2737–2740.

Wasilenko, S. T., Stewart, T. L., Meyers, A. F. & Barry, M. (2003). *Proc. Natl Acad. Sci. USA*, **100**, 14345–14350.

Westphal, D., Ledgerwood, E. C., Hibma, M. H., Fleming, S. B., Whelan, E. M. & Mercer, A. A. (2007). *J. Virol.* **81**, 7178–7188.

White, E., Sabbatini, P., Debbas, M., Wold, W., Kusher, D. I. & Gooding, L. (1992). *Mol. Cell. Biol.* **12**, 2570–2580.

Whitten, A. E., Cai, S. & Trewhella, J. (2008). *J. Appl. Cryst.* **41**, 222–226.

Winn, M. D. *et al.* (2011). *Acta Cryst.* D**67**, 235–242.

Youle, R. J. & Strasser, A. (2008). *Nature Rev. Mol. Cell Biol.* **9**, 47–59.

Yu, E., Zhai, D., Jin, C., Gerlic, M., Reed, J. C. & Liddington, R. (2011). *J. Biol. Chem.* **286**, 30748–30758.

Zhai, D., Yu, E., Jin, C., Welsh, K., Shiau, C., Chen, L., Salvesen, G. S., Liddington, R. & Reed, J. C. (2010). *J. Biol. Chem.* **285**, 5569–5580.